DOI: https://doi.org/10.68732/7b561271008434b8

ISBN: 978-9989-2053-6-1

Fall of Ground Risk Assessment in Underground Excavations Using a Fuzzy Cognitive Rock Engineering System

A. Tursanova, R. Afshar & A. Adoko
School of Mining and Geosciences, Nazarbayev University, Astana, Kazakhstan
amoussou.adoko@nu.edu.kz
0000-0003-1396-7811

Abstract

Fall of Ground (FoG) incidents remain among the most critical safety and operational hazards in underground mining. This study introduces a causality-based Rock Engineering System (RES) for the risk assessment of FoG hazards in underground excavations. A FoG risk index is proposed to systematically quantify the hazard level and evaluate the influence of contributing factors. The RES is weighted using a fuzzy cognitive map (FCM) to reduce subjectivity in determining the interaction matrix of the FoG system. A dataset of over 100 FoG cases from a local underground mine was compiled to develop and validate the FoG risk index. The results indicated that ground support conditions, excavation geometry, and rock fracturing are among the most important parameters controlling FoG occurrence in the mine. The proposed index was compared with the observed FoG size, and the results showed a good correlation (R = 0.78). It is concluded that the proposed index can be effectively used to assess FoG risk in underground excavations.

Keywords

Fall of Ground (FoG), Rock Engineering System (RES), Fuzzy Cognitive Map (FCM), Underground Mining.

1 Introduction

The stability of underground openings remains a critical concern in mining operations. Fall of Ground (FoG) refers to a gravity-driven mining hazard characterized by the detachment of loose rock from excavation surfaces (Peng, 2022). FoG may result from either structural or stress-induced failure and can occur even in supported excavations, posing serious risks to safety, productivity, and profitability of underground mining operations worldwide (Wang et al., 2022). Consequently, effective FoG management requires a comprehensive understanding of the factors controlling the failure mechanisms of the surrounding rock mass.

To improve mine safety and mitigate FoG hazards, numerous assessment approaches have been developed over the past decades, including numerical modelling, empirical methods, expert systems, machine learning, probabilistic techniques, and decision-matrix approaches (Adoko et al., 2019; Isleyen et al., 2021; Małkowski and Juszyński, 2021). Although these methods have significantly enhanced FoG prediction and understanding, many of them still struggle to objectively capture the

complex interactions among the controlling factors. This challenge arises because FoG is inherently a multifactorial problem governed by the interaction of parameters such as rock mass quality, excavation geometry, support systems, groundwater conditions, stress redistribution, and adverse geological structures (Wu et al., 2018; Adoko et al., 2020; Hekmatnejad et al., 2021; Zuo et al., 2024).

Recent advances in rock engineering have therefore emphasized system-based and data-driven approaches for addressing such complexity. Among these, the Rock Engineering Systems (RES) approach provides a structured methodology for analysing complex geotechnical systems through interaction matrices representing relationships among influencing parameters (Hudson, 1992; Salmi et al., 2025). Recent studies suggest that the predictive capability of RES can be further enhanced through integration with intelligent techniques such as Fuzzy Cognitive Maps (FCMs), which enable a more objective quantification of parameter interactions and system weights based on expert knowledge (Zhang et al., 2024). FCMs combine fuzzy logic and neural-network concepts to represent causal reasoning in complex systems (Cosma et al., 2017). Accordingly, this study develops a causality-based RES framework in which FCMs are employed to establish the interaction matrix for FoG hazard assessment in underground excavations.

2 Methodology

2.1 An overview of the RES-FCM

The RES utilizes an interaction matrix to represent causal relationships among parameters controlling a rock engineering problem such as FoG occurrence. The matrix is square, with main factors P_i located along the leading diagonal, while off-diagonal cells encode pairwise interactions I_{ij}. These interactions are conventionally quantified using the Expert Semi-Quantitative (ESQ) coding scheme, which assigns values between 0 (no interaction) and 4 (critical interaction). As shown in Fig. 1a, each row corresponds to the Cause (C_{pi}) of factor P_i, representing its influence on other parameters, while each column corresponds to the Effect (E_{pj}), representing the influence of other parameters on P_i. The cause and effect values are computed as:

$$C_{pi} = \sum_{j=1}^{n} I_{ij}, n \qquad E_{pj} = \sum_{i=1}^{n} I_{ij}, n \tag{1}$$

whereC_{pi} and E_{pj} are the number of columns and rows, respectively.

Once the cause and effect values are obtained, the parameter interaction intensity (PII), calculated as (C+E)/√2, and the parameter dominance (PD), calculated as (C-E)/√2, are employed to characterize the degree and nature of interaction among the parameters.

The overall importance of each factor (weight) is determined by the normalized sum of cause and effect as follows:

$$a_i = \frac{(C_i + E_i)}{(\sum_i C_i + \sum_i E_i)} \times 100 \tag{3}$$

This weighting ensures that both causal and effect contributions are incorporated into the system analysis. The FoG index describing the FoG behaviour is computed as:

$$FoG\ Risk_{index} = \sum a_i V_i \tag{4}$$

In Eq. 4 $V_i$denotes the rating values assigned to each the parameter P_i of FoG system. The values of FoG index can range from 0 to 100. The higher the index value, the greater the FoG risk.

The RES matrix can be used to initialize and then train a Fuzzy Cognitive Map (FCM) topology (see Fig. 1b). In this diagram, nodes (C1,C2,…,Cn) represent the FoG parameters are known as concepts, while directed edges (W_{ij}) denote causal relationships. The FCM update rule is:

$$A_i^t = f\left(A_i^{t-1} + \sum_{j\neq i}^{N} A_j^{t-1} \times W_{ij}\right) \tag{5}$$

whereA^t is the fuzzy value of a concept at iteration t, A^{t-1} is its value in the previous iteration, W_{ij} is connection weight linking concept C_j to concept C_i. This iterative process continues until convergence, allowing dynamic simulation of parameter interactions. After convergence an FCM interaction matrix is obtained.

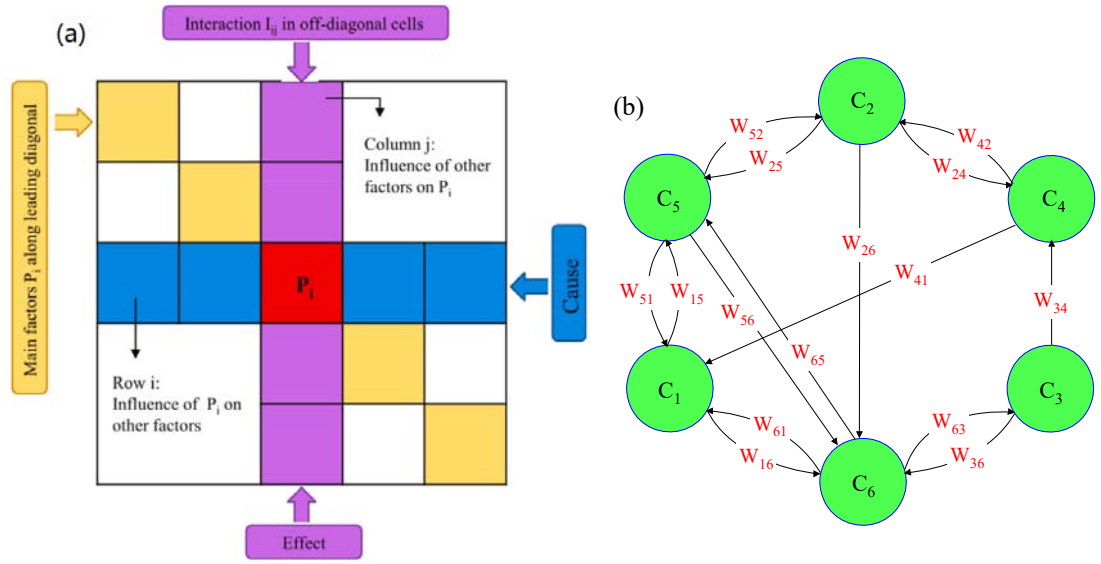


Fig. 1 (a) RES working principle and (b) Graphical representation of FCM topology.

2.2 Data description

In this study, 100 FoG cases from a local underground mine was compiled to develop and validate the FoG risk index model. The dataset contains 13 parameters namely, excavation type (P1), excavation span (P2), excavation height (P3), excavation depth (P4), fault presence (P5), shear zone (P6), groundwater condition (P7), support category (P8), fracture rating (P9), uniaxial compressive strength (P10), friction angle (P11) and geological conditions (P12). The dependent parameter is FoG (P13). A sample of the dataset is shown in Table 1.

Table 1. FoG data sample.

P1	P2	P3	P4	P5	P6	P7	P8	P9	P10	P11	P12	FoG (Tons)
3	5.22	5.15	292.49	0	0	2	2	3	184.7	53.8	1	712.85
2	4.74	4.88	252.09	0	0	0	2	2	184.7	53.8	0	15.9
2	11	6	130	0	0	2	1	2	149.3	59.8	3	195.52
3	17.34	9.89	194.4	1	0	2	3	2	184.7	53.8	4	129.85
3	5.94	5	112	0	1	0	1	2	149.3	59.8	4	388.96
3	10.3	4.76	131	0	0	2	2	2	206.3	60	0	266.22
3	5.3	5.06	337	1	0	3	2	2	184.7	53.8	4	3.38
2	11.3	8.92	204	1	0	0	2	2	184.7	53.8	4	88.4
3	7	5.7	94	0	0	1	1	1	184.7	53.8	1	177.55
3	4.96	4.76	259	0	0	2	3	3	184.7	53.8	3	408.1

3 Results and discussions

First, the interaction matrix based on semi-qualitative encoding was established (Table 2). The interactive intensity, dominance, and cause–effect relationships among the twelve excavation-related parameters are presented in Fig. 2a and Fig. 2b. The results indicate that P8 and P9 exhibit the highest interaction intensities, highlighting their strong influence on excavation stability and fragmentation. In contrast, P1 and P4 show relatively low interaction intensities, suggesting a weaker direct influence within the system.

Regarding dominance, P5 and P6 emerge as the most influential parameters, exerting strong and positive causal effects on other factors, whereas P8 indicates the largest negative dominance. P8 and P9 are more subordinate and largely influenced by external parameters as shown in the cause–effect diagram in Fig. 2b. Parameters located below the equality line (C = E), including P1, P4, P5, P6, and P7, are dominant factors driving FoG occurrence. In contrast, P2, P3, P8, P9, and P12 lie above the line, indicating subordinate behavior and greater dependence on other parameters. Parameters P10 and P11, located near the equality line, exhibit balanced cause–effect relationships and comparatively limited influence within the system. Overall, the analysis demonstrates that structural and geomechanical parameters and support conditions control most the FoG behavior, which is consistent

with FoG mechanism. Subordinate parameters such as support category, groundwater condition, and fracture rating play secondary roles, primarily influenced by dominant factors rather than driving system behaviour.

Table 2. RES matrix used in this study.

P1	**4**	**4**	**0**	**0**	**0**	**0**	**3**	**2**	**0**	**0**	**0**
0	P2	2	0	0	0	1	3	2	0	0	0
0	3	P3	0	0	0	1	2	2	0	0	0
1	2	2	P4	0	0	1	3	3	2	1	1
2	3	3	1	P5	1	2	4	4	2	2	4
2	3	3	0	0	P6	2	4	4	4	4	4
0	1	1	0	0	0	P7	4	4	4	4	4
0	0	0	0	0	0	0	P8	2	0	0	0
1	2	2	0	0	0	2	4	P9	0	0	2
1	1	1	0	0	0	0	4	3	P10	3	3
0	1	1	0	0	0	0	4	4	4	P11	3
1	1	1	0	0	0	0	3	0	0	0	P12

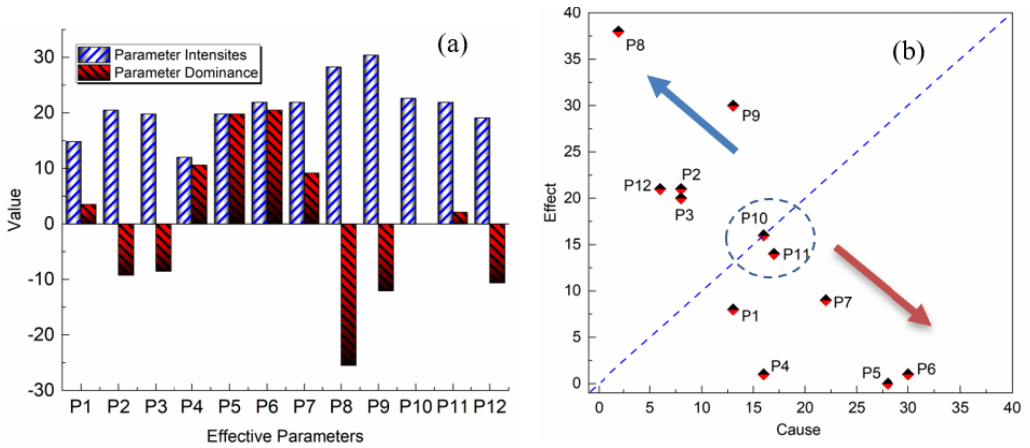


Fig. 2(a) Parameter intensity and dominance; (b) Cause-effect plot for the FoG risk index.

3.1 FCM training

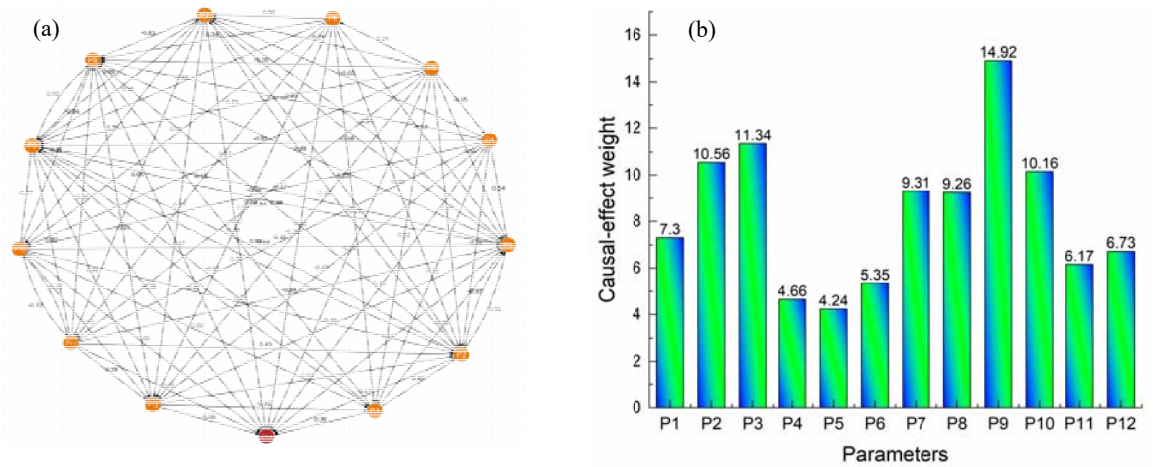


Fig. 3 (a) the structured topology of the map and (b) the resulting final weights of those parameters.

The designed FCM network is shown in Fig. 3(a), while the parameter interaction weights are presented in Fig. 3(b). These weights were obtained through the FCM updating process applied to the initial RES interaction matrix, and the resulting matrix is provided in Table 3. The results indicate that P9 emerges as the most influential parameter, highlighting its critical role in FoG occurrence. Other dominant parameters include P2, P3, and P10, all of which exhibit relatively high cause–effect weights. In contrast, P5 and P6 were found to be less dominant within the FoG system.

The integrated analysis suggests that fracture rating, compressive strength, excavation span, excavation height, groundwater conditions and, support conditions are the primary factors controlling FoG risk in the study area. Conversely, geological structures such as fault zones and shear zones exhibited comparatively lower influence on FoG occurrence.

These findings are somewhat inconsistent with the observed site conditions and therefore constitute a limitation of the present study. Actually, the dominant FoG mechanisms observed at the Mine, included roof subsidence, wedge failures in shear zones, bedding-plane failures, and structurally controlled failures in faulted areas. This discrepancy may be attributed to the use of a training algorithm within the FCM framework combined with the limited size of the available dataset. Future research should therefore focus on expanding the database, incorporating additional influencing factors such as blasting effects on excavations (Imashev et al., 2024), and also accounting for uncertainties in parameter properties (Adoko et al., 2011). Nonetheless, the current results are in agreement with FoG occurrence modes as suggested by previous studies (Małkowski and Juszyński, 2021).

Table 3. Interaction matrix used to initiate the FCM.

P1	**0.599**	**0.250**	**0.000**	**0.000**	**0.000**	**0.000**	**0.358**	**0.469**	**0.000**	**0.000**	**0.000**
0.000	P2	0.966	0.000	0.000	0.000	0.176	0.846	0.203	0.000	0.000	0.000
0.000	0.910	P3	0.000	0.000	0.000	0.951	0.881	0.341	0.000	0.000	0.000
0.208	0.977	0.543	P4	0.000	0.000	0.031	0.205	0.805	0.355	0.156	0.068
0.523	0.235	0.082	0.047	P5	0.243	0.239	0.060	0.229	0.668	0.505	0.259
0.212	0.377	0.118	0.000	0.000	P6	0.898	0.343	0.878	0.556	0.181	0.089
0.000	0.225	0.535	0.000	0.000	0.000	P7	0.807	0.485	0.755	0.054	0.669
0.000	0.000	0.000	0.000	0.000	0.000	0.000	P8	0.988	0.000	0.000	0.000
0.903	0.895	0.766	0.000	0.000	0.000	0.953	0.917	P9	0.000	0.000	0.459
0.862	0.754	0.678	0.000	0.000	0.000	0.000	0.210	0.775	P10	0.374	0.686
0.000	0.428	0.838	0.000	0.000	0.000	0.000	0.157	0.797	0.722	P11	0.277
0.927	0.099	0.395	0.000	0.000	0.000	0.000	0.968	0.000	0.000	0.000	P12

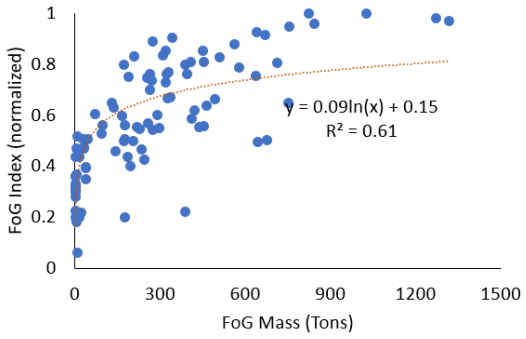


Fig. 4 Comparison between normalized FoG risk index and Observed FoG size.

3.2 Fog index

Finally, the FoG index was calculated for the whole dataset according to Eq. 4. In order to validate the results, the FoG index values were compared with observed FoG size. The results are provided in Fig. 8. As it can be seen, a power function was used to fit the data. A coefficient of correlation of **R = 0.78** (R^2 = 0.61) was obtained, indicating a strong correlation between the proposed index and the actual FoG. The index was scaled into [0,1] for convenience. The FoG size can be estimated using the following empirical relationship:

$$FoG\ Risk_{index} = 0.09 ln FoG + 0.15 \quad (6)$$

4 Conclusion

This study investigated the feasibility of implementing of Rock Engineering System and Fuzzy Cognitive Map methodology to establish a novel index to quantify FoG risk in underground mine excavations. The results showed that fracture rating, compressive strength, excavation span,

excavation height, groundwater conditions and, support conditions are the primary factors controlling FoG risk in the study area. Conversely, geological structures such as fault zones and shear zones exhibited comparatively lower influence on FoG occurrence. In addition, an empirical relationship between the FoG Risk Index and observed FoG conditions yielded a strong correlation coefficient (R= 0.78), demonstrating good agreement with field observations. The results suggest that the FoG Index can serve as a practical tool for FoG hazard assessment, ground control design, and geotechnical risk management. However, the dataset remains limited for broader generalization. Future work should extend the database to additional mining sites and incorporate more parameters.

Acknowledgment

This research was funded by the Science Committee of the Ministry of Science and Higher Education of the Republic of Kazakhstan (Grant No. AP26199097). The authors also wish to acknowledge the valuable contributions of the anonymous reviewers.

References

Adoko, A. C., J. Vallejos and R. Trueman. 2020. Stability assessment of underground mine stopes subjected to stress relaxation. Mining Technology: Transactions of the Institute of Mining and Metallurgy.

Adoko, A. C., M. Zhalel and P. T. Phumaphi. 2019. Fall of ground characterization: A case study of BCL Mine, Botswana. In the Procedings of 53rd U.S. Rock Mechanics/Geomechanics Symposium.

Adoko, A. C., Q.-J. Zuo and L. Wu. 2011. A Fuzzy Model for High-Speed Railway Tunnel Convergence Prediction in Weak Rock. Electronic Journal of Geotechnical Engineering. 16(Q): 1275-1295.

Cosma, G., D. Brown, M. Archer, M. Khan and A. Graham Pockley. 2017. A survey on computational intelligence approaches for predictive modeling in prostate cancer. Expert Systems with Applications. 70: 1-19.

Hekmatnejad, A., B. Crespin, J. A. Vallejos, A. Opazo and A. C. Adoko. 2021. A hybrid predictive model of unstable rock blocks around a tunnel based on estimated volumetric fracture intensity and circular variance from borehole data sets. Tunnelling and Underground Space Technology. 111.

Hudson, J. A. 1992. Rock engineering systems: theory and practice. Chichester, Ellis Horwood.

Imashev, A., A. Mussin and A. C. Adoko. 2024. Investigating an Enhanced Contour Blasting Technique Considering Rock Mass Structural Properties. Applied Sciences. 14(23): 11461.

Isleyen, E., S. Duzgun and R. McKell Carter. 2021. Interpretable deep learning for roof fall hazard detection in underground mines. Journal of Rock Mechanics and Geotechnical Engineering. 13(6): 1246-1255.

Małkowski, P. and D. Juszyński. 2021. Roof fall hazard assessment with the use of artificial neural network. International Journal of Rock Mechanics and Mining Sciences. 143: 104701.

Peng, S. 2022. Roof bolting and underground roof falls. Geohazard Mechanics.

Salmi, E. F., E. J. Sellers and E. Hamman. 2025. Rock Engineering Systems for Quantifying Risks and Controls for the Resilient Design and Optimisation of Long and Ultra-long Ore Passes. Rock Mechanics and Rock Engineering. 58(11): 12359-12418.

Wang, Y. J., L. S. Zhao and Y. S. Xu. 2022. Analysis of Characteristics of Roof Fall Collapse of Coal Mine in Qinghai Province, China. Applied Sciences (Switzerland). 12(3).

Wu, L., A. C. Adoko and B. Li. 2018. An Illustration of Determining Quantitatively the Rock Mass Quality Parameters of the Hoek–Brown Failure Criterion. Rock Mechanics and Rock Engineering. 51(4): 1063-1076.

Zhang, Z., S. Hosseini, M. Monjezi and M. Yari. 2024. Extension of reliability information of Z-numbers and fuzzy cognitive map: Development of causality-weighted rock engineering system to predict and risk assessment of blast-induced rock size distribution. International Journal of Rock Mechanics and Mining Sciences. 178: 105779.

Zuo, Q., X. Li, P. Li, M. Deng and A. C. Adoko. 2024. Surrounding rock instability mechanism for fault-crossing tunnels in water-rich soft rock. Bulletin of Engineering Geology and the Environment. 83(6).